Evolution of Propagating Coherent Pulses Driving a Single Superconducting Artificial Atom

A. V. Vasenin,[1,2,*] Sh. V. Kadyrmetov,[1] A. N. Bolgar,[1] A. Yu. Dmitriev,[1,3] and O. V. Astafiev[2,1]
[1]Laboratory of Artificial Quantum Systems, Moscow Institute of Physics and Technology, 141701 Dolgoprudny, Russia
[2]Skolkovo Institute of Science and Technology, Nobel Street 3, 143026 Moscow, Russia
[3]National University of Science and Technology "MISIS," 119049 Moscow, Russia

(Received 11 September 2023; accepted 3 July 2024; published 14 August 2024)

An electromagnetic wave propagating through a waveguide with a strongly coupled two-level superconducting artificial atom exhibits an evolving superposition with the atom. The Rabi oscillations in the atom result from a single excitation-relaxation, corresponding to photon absorption and stimulated emission from and to the field. In this study, we experimentally investigated the time-dependent behavior of the field transmitted through a waveguide with a strongly coupled transmon. The scattered fields agree well with the predictions of the input-output theory. We demonstrate that the time evolution of the propagating fields, because of the interaction, encapsulates all information about the atom. Furthermore, we deduced the dynamics of the incoherent radiation component from the first-order correlation function of the measured field.

DOI: 10.1103/PhysRevLett.133.073602

Introduction—Waveguide quantum electrodynamics (wQED) involves artificial atoms coupled to the propagating field in a waveguide [1–4]. The possibility to make a strong coupling between a superconducting artificial atom and unconfined field was key to the first successful wQED experiments [5–8]. Subsequently, the focus shifted to more complex systems, for example, several qubits coupled to a waveguide [9–12]. The use of coherent and incoherent emission to infer a qubit state was demonstrated in [13]. Practical applications of qubit-waveguide systems include the creation of efficient single-photon sources [14–16], and the coupling of two distant qubits by a waveguide to observe their entanglement [9,17–19]. Despite several prototypes, the superconducting platform lacks robust gigahertz single-photon detectors [20–22]. However, tomographic methods using linear field detectors can reliably characterize microwave fields emitted by superconducting quantum systems [23,24]. These methods enable the resolution of peculiar properties of resonance fluorescence [25,26], as well as the characterization of numerous non-Gaussian states of light [27] and nonclassical multiphoton states with time-bin entanglement [28].

Despite the aforementioned achievements, there are still gaps in the experimental characterization of nonstationary resonance fluorescence of a two-level atom [29,30]. Researchers mainly study driven two-level systems in the stationary regime, focusing on fluorescence from steady states [5,31] or the time-averaged radiation spectra of pulse-driven atoms [7,32]. Previous attempts to observe the dynamics of the driving field were limited to observing spontaneous emission [33,34], using very short pulses [35–37], or experimenting with collective atomic states [12]. However, none of these works provides a thorough time-domain characterization of the field dynamics when an arbitrarily long propagating pulse interacts with a single atom and then flies away.

In this work, we measured the coherent and incoherent dynamics of the long rectangular propagating microwave pulse that interacts with a single artificial atom (transmon qubit) strongly coupled to the waveguide [38]. We demonstrated that the scattered wave carries information about the atomic evolution because of the atom-field superposition produced from this interaction. Figure 1(a) illustrates a gedankenexperiment, where a rectangular pulse of a coherent field $|\alpha\rangle$ with a carrier frequency that matches the qubit resonance traverses an infinite waveguide. After a certain time, it causes photon absorption and excites the qubit. As a result, the pulse amplitude and power decrease. However, the continuing pulse stimulates the qubit to emit its excitation, thus increasing the pulse amplitude and power higher than their initial magnitudes. These processes repeat until the pulse ends. Decoherence causes the modulating oscillations to decay. After the pulse passes, the qubit state decays into the vacuum of the waveguide, producing an exponential tail [5,13,33]. Our experiments provide insight into the dynamics of a two-level atom fluorescence, including both coherent and incoherent constituents. Estimated parameters of the transmon are: upper sweet spot at 4.9 ± 0.2 GHz, lower at 3.5 ± 0.1 GHz, anharmonicity 350 ± 20 MHz, and T_1 decay time 140 ± 10 ns. The uncertainties take account

*Contact author: vasenin.av@phystech.edu

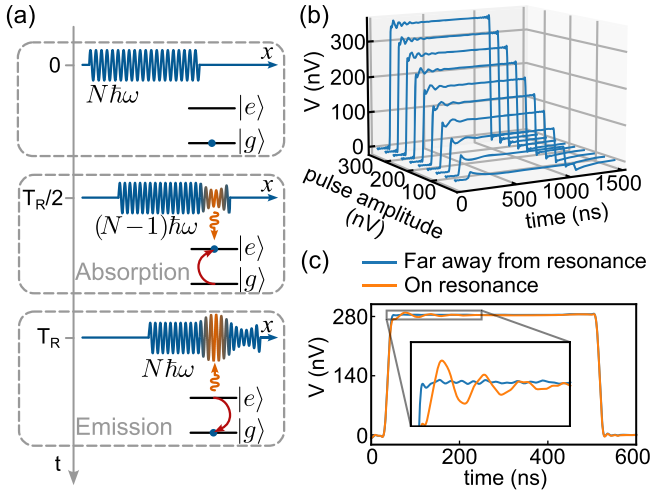

FIG. 1. Stimulated absorption and emission observed in a modulated pulse shape scattered by a two-level atom. (a) Evolution of pulse shape in a waveguide with a two-level atom, showing three stages: a pulse approaching the qubit, photon absorption, and reemission. N represents photon count; $T_R = (2\pi/\Omega_R)$ is the Rabi oscillation period. (b) Voltage traces of the modulated pulse transmitted through a coplanar waveguide with a strongly coupled transmon qubit. (c) Modulation caused by stimulated absorption and emission processes compared to an unmodulated pulse shape. The inset shows an enlarged front part of the pulse. Inset: close-up of the pulse front section.

of the drift in values during several cooling runs of the dilution refrigerator.

Unlike prior methods [13] that utilized repeated pulse sequences to infer qubit states from postpulse spontaneous emission, we directly observe stimulated photon dynamics between the qubit and the field during the pulse drive, extracting Rabi oscillations, qubit population, and the first-order correlation function. The first-order correlation function and instantaneous power density spectra reveal the dynamics of incoherent radiation and confirm the quantum nature of the observed phenomenon. Notably, as the averaged field oscillations diminish, the field correlation function retains its oscillations, highlighting the interplay between coherent and incoherent fluorescence in a nonstationary regime.

Theory—The Hamiltonian of our atom-waveguide system, coupling a two-level atom to one-dimensional waveguide modes, is given by

$$\hat{H} = -\frac{\hbar\omega_q}{2}\hat{\sigma}_z + \sum_{k=l,r}\Big[\int d\omega\hbar\omega\hat{a}^\dagger_{k,\omega}\hat{a}_{k,\omega} + \hbar g\int d\omega\big(\hat{a}_{k,\omega}\hat{\sigma}_+ + \hat{a}^\dagger_{k,\omega}\hat{\sigma}_-\big)\Big], \quad (1)$$

where $\hbar\omega_q$ is the qubit energy, l and r are indices for the left and right modes, g is the coupling constant, $\hat{\sigma}_z$, $\hat{\sigma}_+$, and $\hat{\sigma}_-$ are Pauli operators, and $\hat{a}_{k,\omega}$ is the field annihilation operator.

In our experiments, we measured the field of the right-moving mode. According to input-output theory for tightly coupled atom-waveguide systems [42–46] in the interaction picture, the right output field $\hat{a}_o(t)$ relates to the left input field $\hat{a}_i(t)$ as

$$\hat{a}_o(t) = \hat{a}_i(t) + i\sqrt{\frac{\Gamma_1}{2}}\hat{\sigma}_-(t), \quad (2)$$

where Γ_1 denotes the relaxation rate.

We use IQ mixers that down-convert the signal and produce two field quadratures: $\hat{V}_I(t) = V_0[\hat{a}_o(t) + \hat{a}^\dagger_o(t)]/2$ and $\hat{V}_Q(t) = -iV_0[\hat{a}_o(t) - \hat{a}^\dagger_o(t)]/2$. Here, $V_0 = \sqrt{G\hbar\omega Z_0}$, where G represents the amplification coefficient and Z_0 is the waveguide impedance. Together, they define the full output field $\hat{V}_o(t) = V_I(t) + iV_Q(t) = V_0\hat{a}_o(t)$.

For a coherent ($|\alpha(t)\rangle$) rectangular pulse driving an atom, the state of the atom displays Rabi oscillations at frequency $\Omega_R(t) = \sqrt{2\Gamma_1}\alpha(t)$ [47]. These oscillations, notable during the initial pumping $0 \le t \lesssim 1/\Gamma_1$, manifest in the averaged output voltage trace:

$$\langle\hat{V}_o(t)\rangle = V_0\big(\alpha(t) + i\sqrt{\Gamma_1/2}\langle\hat{\sigma}_-(t)\rangle\big). \quad (3)$$

From Eq. (2), it can be derived that the energy absorbed from the transmitted pulse in the first half of the Rabi period nearly matches the single-photon energy. The same applies to the energy emitted in the subsequent half-cycle. In contrast, the energy reflected in the left direction is minimal. Analytical calculations are detailed in [38].

The nonstationary first-order correlation function can be computed according to the formula

$$G^{(1)}(t_1,t_2) = V_0^2(\langle\hat{a}^\dagger_o(t_1)\hat{a}_o(t_2)\rangle - \langle\hat{a}^\dagger_o(t_1)\rangle\langle\hat{a}_o(t_2)\rangle). \quad (4)$$

While $\langle\hat{V}_o(t)\rangle$ reveals the dynamics of the coherent part of the radiation, $G^{(1)}(t_1,t_2)$ exposes the dynamics of the incoherent component of the field [38].

The first-order correlation function highlights the property of the $\hat{a}$ operator in preserving a coherent state, such as $\hat{a}|\alpha\rangle = \alpha|\alpha\rangle$, and the role of $\hat{a}^\dagger$ in disrupting coherence [48]. Assuming $\alpha(t)g\delta t \ll 1$, the evolution operator $\hat{U}(t,t+\delta t)$ is approximated as $1 - ig\delta t[\hat{a}(t)\hat{\sigma}_+ + \hat{a}^\dagger(t)\hat{\sigma}_-]$. Its action on the atom-field wave function $|\Psi_q(t),\alpha(t)\rangle$ preserves or spoils the coherent state of the field, depending on the state of the qubit. For example, if

$$\hat{U}(t,t+\delta t)|g\rangle|\alpha(t)\rangle \approx (|g\rangle - ig\alpha(t)\delta t|e\rangle)|\alpha(t)\rangle, \quad (5)$$

the state is preserved. However, it is disrupted if

$$\hat{U}(t,t+\delta t)|e\rangle|\alpha(t)\rangle \approx (|e\rangle|\alpha(t)\rangle - ig\delta t|g\rangle\hat{a}^\dagger(t)|\alpha(t)\rangle). \quad (6)$$

In this context, when the qubit is in an excited state, the evolution operator applies $\hat{a}^\dagger$ to the field state, potentially

destroying its coherence. Using these states (5) and (6) in conjunction with (4), one can demonstrate that $G^{(1)}(t_1,t_1+\tau)\approx 0$ at $t_1=(2\pi n/\Omega_R)$ and $G^{(1)}(t_2,t_2+\tau)\neq 0$ at $t_2=[\pi(2n-1)/\Omega_R]$, as corroborated by our experiments.

Results and discussion—We first measure the average voltage trace of a rectangular pulse on resonance with the qubit. The effect of the spectral width of the pulse is discussed in the Supplemental Material [38]. Figure 1(b) shows oscillations near the front of the pulse, which increase in frequency with pulse amplitude while maintaining their amplitude consistent. In Fig. 1(c), comparing the pulse shape when the qubit is on resonance and far-detuned reveals that modulation begins with a decrease in pulse amplitude, likely signifying photon absorption. To further investigate this modulation, we subtract the two measurements.

Figure 2(a) shows such differences for a resonant case (traces RR, RI) and a slightly off-resonant case (traces NR, NI) when the carrier frequency deviated from the qubit frequency. We measure and digitally rotate two quadratures of the field so that the real quadrature is in phase with the pulse and the imaginary quadrature has an orthogonal phase. Resonant real (RR) and imaginary (RI) quadrature traces display oscillations during the pulse drive and an exponential decay postpulse. The simulation of $\langle\hat{\sigma}_-(t)\rangle$ identifies these traces as Rabi oscillations. Their magnitude spectra are shown in Fig. 2(d), with the horizontal axis centered at the pulse carrier frequency. A sharp peak in the spectra corresponds to postpulse exponential decay of the radiation field and matches the qubit frequency, while the two wide peaks represent positive and negative Rabi frequencies in the resonant trace. For the nonresonant trace, the right peak aligns with the positive Rabi frequency, and the left peak is at 0 Hz, indicating a constant voltage offset during the pulse, visible in Fig. 2(a) (trace NI).

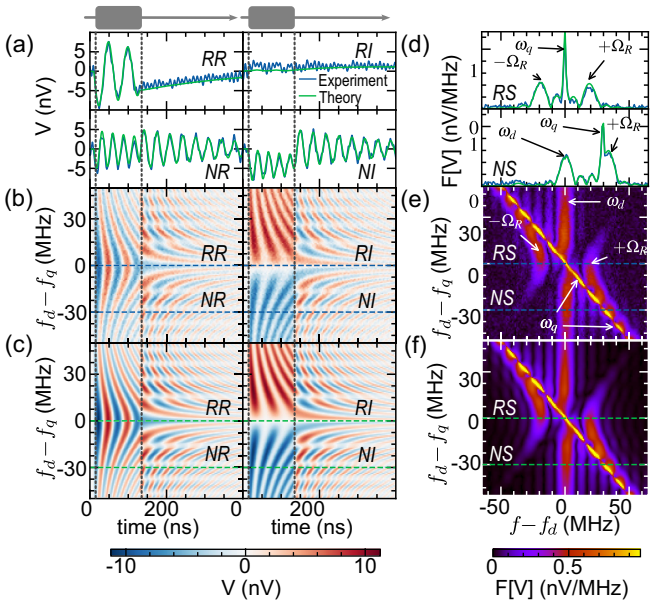

FIG. 2. Radiation of a qubit versus detuning of a pulse carrier frequency (ω_d) from the qubit transition frequency (ω_q), where radiation is the difference between a modulated pulse and an unperturbed pulse. The pulse is rectangular with 120 ns length. (a) Single radiation traces for resonant and slightly off-resonant (-30 MHz) cases. Left (right) columns represent the real (imaginary) parts. (b) Experimental traces plotted in color as a function of detuning. (c) Simulation results for radiation traces. (d) Magnitude spectra (RS and NS) of the single traces taken from (a). The arrows show Rabi, qubit, and drive frequencies. (e) Experimental spectra plotted in color as a function of detuning. (f) Simulated spectra plotted in color. Vertical dashed lines mark the region where the pulse drives the qubit, and the horizontal dashed lines correspond to the traces in (a). The dashed lines in (e) and (f) link to the spectra in (d). Labels: R for resonant, N for nonresonant, followed by R for real, I for imaginary, and S for spectrum.

Traces were scanned by varying the pulse frequency f_d around the set qubit frequency f_q. The experimental results and simulations are shown in Figs. 2(b) and 2(c), with magnitude spectra in Figs. 2(e) and 2(f). Fitting data yielded the following qubit parameters: qubit frequency $f_q = 4.835$ GHz, Rabi frequency $\Omega_R/(2\pi) = 20.1$ MHz, decay rate $\Gamma_1/(2\pi) = 1.4$ MHz, and dephasing rate $\gamma/(2\pi) = 0.5$ MHz. This measurement was not performed at the qubit sweet spot because of a spurious two-level system, hence the large dephasing. Figures 2(b) and 2(c) reveal two regions: the first is the qubit radiation during the microwave drive that yields three spectral peaks at $f_d - \Omega/(2\pi)$, f_d, and $f_d + \Omega/(2\pi)$ where $\Omega = \sqrt{\Omega_R^2 + \delta^2}$ and $\delta = 2\pi(f_d - f_q)$. Their width is mostly defined by the pulse length. The second is the spontaneous emission postpulse [33], which yields a peak limited by Γ_2, consistent with the qubit frequency as the carrier shifts. With a known Rabi frequency and decay rate, the voltages were recalibrated to the values radiated by the artificial atom on the chip [47]. The asymmetry of the peak amplitudes with respect to the driving frequency can be explained by the asymmetry of the transition amplitudes in the dressed-state basis [38].

The first-order correlation function $G^{(1)}(t_1,t_2)$ for a finite-length pulse was measured using Eq. (4) and methods from [15,49]. Figure 3(c) shows the real part of Eq. (4) for the resonant case, while Fig. 3(d) displays 1D slices of the correlation function, indicating that the imaginary part is close to zero. The mesh-patterned square in Fig. 3(c) highlights correlations during the pulse drive, with primarily real positive values in both resonant and nonresonant scenarios (see Ref. [38]). The fading area of the other square along the diagonal corresponds to postpulse correlations, real and positive only in resonance. The rectangles flanking the diagonal show voltage correlations between pulse and postpulse times. The real positive nature of the function during the pulse underscores the quantum nature of the effect, since classical coherent oscillating fields

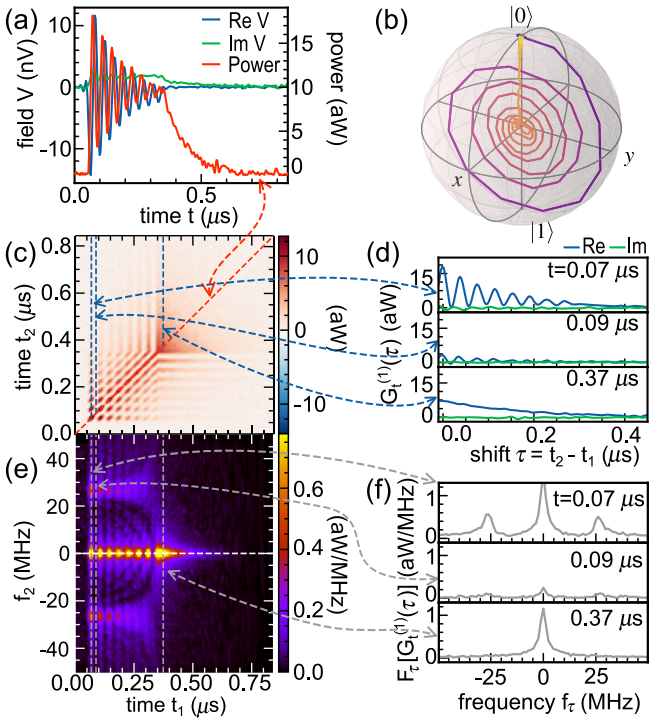

FIG. 3. Measurement of the second-order momenta of the field in the resonant case. The driving pulse is rectangular with 300 ns length. (a) Traces of field and radiated power. Field traces correspond to $\langle\sigma_x\rangle$ and $\langle\sigma_y\rangle$, while radiated power reflects qubit population. (b) Qubit state evolution extracted from traces in (a). (c) Real part of the first-order correlation function. Its diagonal trace is the power trace in (a). Vertical slices are shown in (d). (e) Fourier spectra taken along $\tau = t_2 - t_1 > 0$ for the first-order correlation function. Vertical slices from (e) are shown in (f).

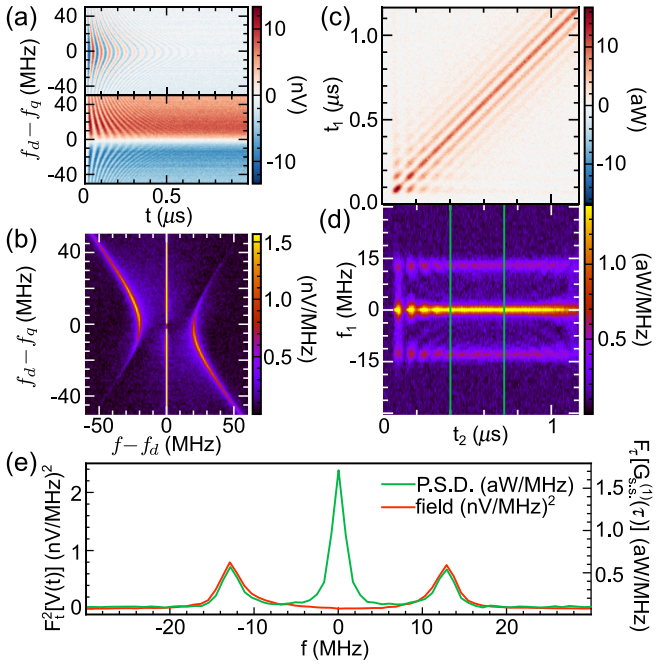

FIG. 4. Properties of qubit radiation during a long pulse with a large amplitude. The driving pulse is rectangular with 1500 ns length. (a),(b) Dynamics of the coherent field and its spectra as a function of the frequency difference between the qubit resonance and the carrier frequency. (c),(d) Nonstationary two-time first-order correlation function and instant power spectral density (P.S.D.) for the pulse on resonance. (e) Comparison of the squared spectrum of the average field with the power spectral density in the steady state, which exhibits a Mollow triplet. To smooth the P.S.D. we averaged it over the stationary period between the two green lines in subfigure (d).

cannot exhibit the same property. Additionally, the averaged field, combined with the diagonal trace of the correlation function [Fig. 3(a)], provides a complete tomography of the qubit state evolution [Fig. 3(b)]. In this figure, we assumed a temperature of 0 K. From comparing spectroscopy data to numerical simulations, the thermal population of the first excited level is observed to be smaller than 2%–3%, resulting in an error on the inferred qubit states of 4%–6% [38].

To analyze the measured $G^{(1)}(t_1, t_2)$, a Fourier transform is performed as

$$\mathrm{IPSD} = \left| \int_0^{+\infty} G^{(1)}(t, t+\tau) e^{-i\omega\tau} d\tau \right|, \qquad (7)$$

with $\tau = t_2 - t_1 > 0$ representing the time difference between two points. The IPSD (instant power spectral density) reveals three distinct peaks [Figs. 3(e) and 3(f)] during the pulse drive, with sidebands at Rabi frequencies. Postpulse, only the central peak remains, related to spontaneous emission.

A long-pulse measurement [see Figs. 4(a) and 4(c) for the 1000 ns pulse, exceeding the depicted region] improves the spectral resolution. The stimulated emission peaks in the field spectra [Fig. 4(b)] become narrower, constrained by $(\Gamma_1 + \Gamma_2)/2$. At $\omega_d \neq \omega_q$, there are two peaks at $f = f_d$, a bright narrow peak on top of a broad smeared peak with width $\Gamma_2/2$. The free-decay spectral line is absent in Fig. 4(b) because we have cut voltage traces at the end of the pulse. Figure 4(c) depicts the real part of the first-order correlation function for the in-resonance case, covering the transient region and the steady state region $t > 0.5$ μs, where the qubit state oscillations have faded. In this steady region, the correlation function oscillates with the time difference $\tau = t_2 - t_1$. Fourier transformation along τ and averaging within the steady region [between the green lines in Fig. 4(d)] produces a power spectral density (PSD) similar to a Mollow triplet [5,50]. Comparison with the squared spectrum of the averaged field in resonance [Fig. 4(e)] shows that the sidebands align, while the central peak is absent as a result of interference between the two resonant transitions in the dressed atom picture.

As discussed in the theory section, our results [Figs. 3(c)–3(f)] demonstrate that $G^{(1)}(t, t+\tau)$ approaches zero for any τ at times t between two adjacent Rabi periods,

while it is nonzero at other time points. For example, all the peaks in IPSD [Figs. 3(e) and 4(d)] exhibit oscillations with Rabi frequency along the t_1 axis. In Figs. 4(c) and 4(d), it is also observed that the decoherence gradually diminishes the initially coherent Rabi oscillations for a very long pulse, as time progresses beyond $t > 1/\Gamma_1$ where $G^{(1)}(t, t+\tau)$ no longer turns zero.

Conclusion—We have measured the coherent and incoherent field dynamics of a propagating rectangular microwave pulse that has interacted with a superconducting artificial atom. Previous quantum optical experiments mainly observed the exponential tail postpulse, which encapsulates the energy of a photon over an extended decay time. Yet, within the pulse, the qubit also absorbs and emits photons. Given the swift Rabi oscillations, this photon energy is confined to a briefer span, resulting in power oscillations of greater amplitude than the exponential tail. Thus, besides the fundamental quantum optics research, qubit state measurements can also benefit from measuring the modulation of a driving pulse after interaction with the atom.

Acknowledgments—We acknowledge the support of the Russian Science Foundation (Grant No. 23-72-01052). This work was carried out using equipment from the MIPT Shared Facilities Center.

[1] I.-C. Hoi, C. M. Wilson, G. Johansson, J. Lindkvist, B. Peropadre, T. Palomaki, and P. Delsing, Microwave quantum optics with an artificial atom in one-dimensional open space, New J. Phys. **15**, 025011 (2013).

[2] X. Gu, A. F. Kockum, A. Miranowicz, Y.-x. Liu, and F. Nori, Microwave photonics with superconducting quantum circuits, Phys. Rep. **718–719**, 1 (2017).

[3] D. Roy, C. M. Wilson, and O. Firstenberg, Colloquium: Strongly interacting photons in one-dimensional continuum, Rev. Mod. Phys. **89**, 021001 (2017).

[4] A. F. Kockum, Quantum optics with giant atoms—the first five years, in *International Symposium on Mathematics, Quantum Theory, and Cryptography* (Springer, Singapore, 2020), pp. 125–146.

[5] O. Astafiev, A. M. Zagoskin, A. A. Abdumalikov, Y. A. Pashkin, T. Yamamoto, K. Inomata, Y. Nakamura, and J. S. Tsai, Resonance fluorescence of a single artificial atom, Science **327**, 840 (2010).

[6] O. V. Astafiev, A. A. Abdumalikov, A. M. Zagoskin, Y. A. Pashkin, Y. Nakamura, and J. S. Tsai, Ultimate on-chip quantum amplifier, Phys. Rev. Lett. **104**, 183603 (2010).

[7] A. A. Abdumalikov, O. Astafiev, A. M. Zagoskin, Y. A. Pashkin, Y. Nakamura, and J. S. Tsai, Electromagnetically induced transparency on a single artificial atom, Phys. Rev. Lett. **104**, 193601 (2010).

[8] I.-C. Hoi, C. M. Wilson, G. Johansson, T. Palomaki, B. Peropadre, and P. Delsing, Demonstration of a single-photon router in the microwave regime, Phys. Rev. Lett. **107**, 073601 (2011).

[9] A. F. van Loo, A. Fedorov, K. Lalumière, B. C. Sanders, A. Blais, and A. Wallraff, Photon-mediated interactions between distant artificial atoms, Science **342**, 1494 (2013).

[10] B. Kannan, M. J. Ruckriegel, D. L. Campbell, A. F. Kockum, J. Braumüller, D. K. Kim, M. Kjaergaard, P. Krantz, A. Melville, B. M. Niedzielski, A. Vepsäläinen, R. Winik, J. L. Yoder, F. Nori, T. P. Orlando, S. Gustavsson, and W. D. Oliver, Waveguide quantum electrodynamics with superconducting artificial giant atoms, Nature (London) **583**, 775 (2020).

[11] B. Kannan, D. L. Campbell, F. Vasconcelos, R. Winik, D. K. Kim, M. Kjaergaard, P. Krantz, A. Melville, B. M. Niedzielski, J. L. Yoder, T. P. Orlando, S. Gustavsson, and W. D. Oliver, Generating spatially entangled itinerant photons with waveguide quantum electrodynamics, Sci. Adv. **6**, eabb8780 (2020).

[12] R. Pennetta, M. Blaha, A. Johnson, D. Lechner, P. Schneeweiss, J. Volz, and A. Rauschenbeutel, Collective radiative dynamics of an ensemble of cold atoms coupled to an optical waveguide, Phys. Rev. Lett. **128**, 073601 (2022).

[13] A. A. Abdumalikov, O. V. Astafiev, Y. A. Pashkin, Y. Nakamura, and J. S. Tsai, Dynamics of coherent and incoherent emission from an artificial atom in a 1d space, Phys. Rev. Lett. **107**, 043604 (2011).

[14] Z. H. Peng, S. E. de Graaf, J. S. Tsai, and O. V. Astafiev, Tuneable on-demand single-photon source in the microwave range, Nat. Commun. **7**, 12588 (2016).

[15] Y. Zhou, Z. Peng, Y. Horiuchi, O. V. Astafiev, and J. S. Tsai, Tunable microwave single-photon source based on transmon qubit with high efficiency, Phys. Rev. Appl. **13**, 034007 (2020).

[16] Y. Lu, A. Bengtsson, J. J. Burnett, B. Suri, S. R. Sathyamoorthy, H. R. Nilsson, M. Scigliuzzo, J. Bylander, G. Johansson, and P. Delsing, Quantum efficiency, purity and stability of a tunable, narrowband microwave single-photon source, npj Quantum Inf. **7**, 140 (2021).

[17] P. Kurpiers, P. Magnard, T. Walter, B. Royer, M. Pechal, J. Heinsoo, Y. Salathé, A. Akin, S. Storz, J.-C. Besse, S. Gasparinetti, A. Blais, and A. Wallraff, Deterministic quantum state transfer and remote entanglement using microwave photons, Nature (London) **558**, 264 (2018).

[18] P. Magnard, S. Storz, P. Kurpiers, J. Schär, F. Marxer, J. Lütolf, T. Walter, J.-C. Besse, M. Gabureac, K. Reuer, A. Akin, B. Royer, A. Blais, and A. Wallraff, Microwave quantum link between superconducting circuits housed in spatially separated cryogenic systems, Phys. Rev. Lett. **125**, 260502 (2020).

[19] S. Storz *et al.*, Loophole-free bell inequality violation with superconducting circuits, Nature (London) **617**, 265 (2023).

[20] K. Inomata, Z. Lin, K. Koshino, W. D. Oliver, J.-S. Tsai, T. Yamamoto, and Y. Nakamura, Single microwave-photon detector using an artificial Λ-type three-level system, Nat. Commun. **7**, 12303 (2016).

[21] S. Kono, K. Koshino, Y. Tabuchi, A. Noguchi, and Y. Nakamura, Quantum non-demolition detection of an itinerant microwave photon, Nat. Phys. **14**, 546 (2018).

[22] J.-C. Besse, S. Gasparinetti, M. C. Collodo, T. Walter, P. Kurpiers, M. Pechal, C. Eichler, and A. Wallraff, Single-shot quantum nondemolition detection of individual itinerant microwave photons, Phys. Rev. X **8**, 021003 (2018).

[23] F. Mallet, M. A. Castellanos-Beltran, H. S. Ku, S. Glancy, E. Knill, K. D. Irwin, G. C. Hilton, L. R. Vale, and K. W. Lehnert, Quantum state tomography of an itinerant squeezed microwave field, Phys. Rev. Lett. **106**, 220502 (2011).
[24] C. Eichler, D. Bozyigit, C. Lang, L. Steffen, J. Fink, and A. Wallraff, Experimental state tomography of itinerant single microwave photons, Phys. Rev. Lett. **106**, 220503 (2011).
[25] P. Campagne-Ibarcq, L. Bretheau, E. Flurin, A. Auffèves, F. Mallet, and B. Huard, Observing interferences between past and future quantum states in resonance fluorescence, Phys. Rev. Lett. **112**, 180402 (2014).
[26] D. M. Toyli, A. W. Eddins, S. Boutin, S. Puri, D. Hover, V. Bolkhovsky, W. D. Oliver, A. Blais, and I. Siddiqi, Resonance fluorescence from an artificial atom in squeezed vacuum, Phys. Rev. X **6**, 031004 (2016).
[27] M. Kudra, M. Kervinen, I. Strandberg, S. Ahmed, M. Scigliuzzo, A. Osman, D. P. Lozano, M. O. Tholén, R. Borgani, D. B. Haviland, G. Ferrini, J. Bylander, A. F. Kockum, F. Quijandría, P. Delsing, and S. Gasparinetti, Robust preparation of Wigner-negative states with optimized snap-displacement sequences, PRX Quantum **3**, 030301 (2022).
[28] P. Kurpiers, M. Pechal, B. Royer, P. Magnard, T. Walter, J. Heinsoo, Y. Salathé, A. Akin, S. Storz, J.-C. Besse, S. Gasparinetti, A. Blais, and A. Wallraff, Quantum communication with time-bin encoded microwave photons, Phys. Rev. Appl. **12**, 044067 (2019).
[29] B. Renaud, R. M. Whitley, and C. R. Stroud, Nonstationary two-level resonance fluorescence, J. Phys. B **10**, 19 (1977).
[30] J. H. Eberly, C. V. Kunasz, and K. Wodkiewicz, Time-dependent spectrum of resonance fluorescence, J. Phys. B **13**, 217 (1980).
[31] Y. Lu, A. Bengtsson, J. J. Burnett, E. Wiegand, B. Suri, P. Krantz, A. F. Roudsari, A. F. Kockum, S. Gasparinetti, G. Johansson *et al.*, Characterizing decoherence rates of a superconducting qubit by direct microwave scattering, npj Quantum Inf. **7**, 35 (2021).
[32] S. Liu, C. Gustin, H. Liu, X. Li, Y. Yu, H. Ni, Z. Niu, S. Hughes, X. Wang, and J. Liu, Dynamic resonance fluorescence in solid-state cavity quantum electrodynamics, Nat. Photonics **18**, 318 (2024).
[33] A. Sharafiev, M. L. Juan, O. Gargiulo, M. Zanner, S. Wögerer, J. J. García-Ripoll, and G. Kirchmair, Visualizing the emission of a single photon with frequency and time resolved spectroscopy, Quantum **5**, 474 (2021).
[34] S. A. Gunin, A. Y. Dmitriev, A. V. Vasenin, K. S. Tikhonov, G. P. Fedorov, and O. V. Astafiev, Quantum and classical field scattered on a single two-level system, Phys. Rev. A **108**, 033723 (2023).
[35] A. Y. Dmitriev, R. Shaikhaidarov, V. N. Antonov, T. Hönigl-Decrinis, and O. V. Astafiev, Quantum wave mixing and visualisation of coherent and superposed photonic states in a waveguide, Nat. Commun. **8**, 1352 (2017).
[36] A. Y. Dmitriev, R. Shaikhaidarov, T. Honigl-Decrinis, S. E. de Graaf, V. N. Antonov, and O. V. Astafiev, Probing photon statistics of coherent states by continuous wave mixing on a two-level system, Phys. Rev. A **100**, 013808 (2019).
[37] A. V. Vasenin, A. Y. Dmitriev, S. V. Kadyrmetov, A. N. Bolgar, and O. V. Astafiev, Dynamics of multiphoton scattering in a two-level mixer, Phys. Rev. A **106**, L041701 (2022).
[38] See Supplemental Material at http://link.aps.org/supplemental/10.1103/PhysRevLett.133.073602 for measurement details, measurement setup, qubit parameters fit, impact of pulse spectral width and finite temperature, measurement results of the nonresonant first-order correlation function, derivation of formulas for the energy absorbed and emitted by the atom, constants in the input-output expression and methods to find average number of photons in the pulse, which includes Refs. [39–41].
[39] Y. Lu, N. Lambert, A. F. Kockum, K. Funo, A. Bengtsson, S. Gasparinetti, F. Nori, and P. Delsing, Steady-state heat transport and work with a single artificial atom coupled to a waveguide: Emission without external driving, PRX Quantum **3**, 020305 (2022).
[40] C. Cohen-Tannoudji, J. Dupont-Roc, and G. Grynberg, *Atom—Photon Interactions* (Wiley, New York, 1998).
[41] C. Gardiner and P. Zoller, *Quantum Noise: A Handbook of Markovian and Non-Markovian Quantum Stochastic Methods with Applications to Quantum Optics* (Springer Science & Business Media, New York, 2004).
[42] C. W. Gardiner and M. J. Collett, Input and output in damped quantum systems: Quantum stochastic differential equations and the master equation, Phys. Rev. A **31**, 3761 (1985).
[43] S. Fan, Ş. E. Kocabaş, and J.-T. Shen, Input-output formalism for few-photon transport in one-dimensional nanophotonic waveguides coupled to a qubit, Phys. Rev. A **82**, 063821 (2010).
[44] B. Peropadre, J. Lindkvist, I.-C. Hoi, C. M. Wilson, J. J. Garcia-Ripoll, P. Delsing, and G. Johansson, Scattering of coherent states on a single artificial atom, New J. Phys. **15**, 035009 (2013).
[45] K. Lalumière, B. C. Sanders, A. F. van Loo, A. Fedorov, A. Wallraff, and A. Blais, Input-output theory for waveguide QED with an ensemble of inhomogeneous atoms, Phys. Rev. A **88**, 043806 (2013).
[46] J. Lindkvist and G. Johansson, Scattering of coherent pulses on a two-level system–single-photon generation, New J. Phys. **16**, 055018 (2014).
[47] T. Honigl-Decrinis, R. Shaikhaidarov, S. E. de Graaf, V. N. Antonov, and O. V. Astafiev, Two-level system as a quantum sensor for absolute calibration of power, Phys. Rev. Appl. **13**, 024066 (2020).
[48] G. S. Agarwal and K. Tara, Nonclassical properties of states generated by the excitations on a coherent state, Phys. Rev. A **43**, 492 (1991).
[49] M. P. da Silva, D. Bozyigit, A. Wallraff, and A. Blais, Schemes for the observation of photon correlation functions in circuit QED with linear detectors, Phys. Rev. A **82**, 043804 (2010).
[50] B. R. Mollow, Power spectrum of light scattered by two-level systems, Phys. Rev. **188**, 1969 (1969).